A comparison of the $R_h = ct$ and ΛCDM cosmologies based on the observed halo mass function

Manoj K. Yennapureddy[1,a], **Fulvio Melia**[2,3,b]

[1] Department of Physics, The University of Arizona, Tucson, AZ 85721, USA
[2] The Applied Math Program, Department of Physics, The University of Arizona, Tucson, AZ 85721, USA
[3] Department of Astronomy, The University of Arizona, Tucson, AZ 85721, USA

Abstract The growth of structure may be traced via the redshift-dependent halo mass function. This quantity probes the re-ionization history and quasar abundance in the Universe, constituting an important probe of the cosmological predictions. Halos are not directly observable, however, so their mass and evolution must be inferred indirectly. The most common approach is to presume a relationship with galaxies and halos. Studies based on the assumption of a constant halo to stellar mass ratio M_h/M_* (extrapolated from $z \lesssim 4$) reveal significant tension with ΛCDM – a failure known as "The Impossibly Early Galaxy Problem". But whether this ratio evolves or remains constant through redshift $4 \lesssim z \lesssim 10$ is still being debated. To eliminate the tension with ΛCDM, it would have to change by about 0.8 dex over this range, an issue that may be settled by upcoming observations with the James Webb Space Telescope. In this paper, we explore the possibility that this major inconsistency may instead be an indication that the cosmological model is not completely correct. We study this problem in the context of another Friedmann–Lemaître–Robertson–Walker (FLRW) model known as the $R_h = ct$ universe, and use our previous measurement of σ_8 from the cosmological growth rate, together with new solutions to the Einstein–Boltzmann equations, to interpret these recent halo measurements. We demonstrate that the predicted mass and redshift dependence of the halo distribution in $R_h = ct$ is consistent with the data, even assuming a constant M_h/M_* throughout the observed redshift range ($4 \lesssim z \lesssim 10$), contrasting sharply with the tension in ΛCDM. We conclude that – if M_h/M_* turns out to be constant – the massive galaxies and their halos must have formed earlier than is possible in ΛCDM.

F. Melia: John Woodruff Simpson Fellow.

[a] e-mail: manojy@email.arizona.edu
[b] e-mail: fmelia@email.arizona.edu

1 Introduction

The central principle behind the theory of structure formation is that large-scale assemblies, such as galaxies and clusters, formed via the growth of gravitational instabilities in the primordial density field, comprised of dark matter, radiation and baryonic matter. By assumption, dark matter is weakly interacting, so it decoupled from the radiation quite early and its fluctuations grew gravitationally to form the halos. Baryonic matter subsequently accreted into these potential wells once it also decoupled from the radiation, forming bound objects that would become stars and galaxies. Although this latter process is not yet fully understood, there is better consensus concerning the halo evolution itself, codified through the so-called halo mass function [1–3]. As it turns out, the halo mass function is highly sensitive to the cosmological parameters in ΛCDM, including the mass fraction Ω_m, the dark energy equation of state parameter w_{de}, and σ_8 [4] – at least at lower redshifts (i.e., $z \lesssim 2$), where it plays a vital role in constraining standard cosmology. At higher redshifts, the halo mass function plays a vital role in probing the re-ionization history of the Universe [5] and the quasar abundance and formation sites [6]. It goes without saying that constraining and evaluating the halo mass function is therefore critical to the evaluation of structure formation in the Universe.

The standard model predicts a rapid evolution in the number density of massive halos throughout the redshift range $10 \gtrsim z \gtrsim 4$. If a strong connection exists between the halos and galaxies they host, one should expect to see a comparably rapid evolution in the number density of galaxies via their luminosity and mass distributions, implying that one should see in ΛCDM a sharp decline in the number density of luminous galaxies at constant luminosity, or a rapid decrease in luminosity for a fixed number density, towards high redshifts. Although the halo mass function has been evaluated using numerical and N-body simulations at high

redshifts, only recently has it been tested observationally. The halos themselves are not directly observable, so they must be probed indirectly, e.g., through the measured galaxy mass distribution assuming a close relationship between the two.

Data gathered recently with the Cosmic Assembly Near-Infrared Deep Extragalactic Survey (CANDELS; [7]), and the Spitzer Large Area Surveys (SPLASH; [8]), allow us to now infer the halo mass function and its evolution with redshift. Past analyses of the halo mass function and galaxy luminosity function from these surveys have generated significant tension between the observations and predictions in the context of ΛCDM [9]. These studies derived the halo mass from the UV luminosity function by assuming a relationship between UV luminosity and stellar mass which was then used to infer the halo mass function assuming another relationship between the stellar mass and halo mass. The outcome of this work [10] indicated that the halo to stellar mass ratio is constant throughout the redshift range $0 \lesssim z \lesssim 4$, but it is not yet clear whether this ratio evolves or remains constant at $z \gtrsim 4$.

In their analysis, Behroozi et al. [11], Behroozi & Silk [12] and Finkelstein et al. [13] concluded that in order to alleviate the tension with ΛCDM, this ratio needs to evolve by as much as ~ 0.8 dex. An opposing view [9,14,15] maintains that such an evolution is not supported by existing data, and that this ratio is instead roughly constant at redshifts $4 \lesssim z \lesssim 10$, continuing the trend seen at $z \lesssim 4$. In this case, the halo distribution would be inconsistent with ΛCDM by at least 2–4 orders of magnitude at redshifts $4 \lesssim z \lesssim 10$, a disparity termed as "The Impossibly Early Galaxy Problem" [9]. It is anticipated that future observations with the NIRCam and NIRspec on the James Webb Space Telescope may settle this debate.

In this paper, we consider what would happen if this problem turns out to be real and provide a possible solution using a recently completed study of the perturbation growth in the $R_{\rm h} = ct$ universe [16] to describe and report the growth of structure from redshift $z \sim 10^{11}$ to 0 in this alternative Friedmann–Lemaître–Robertson–Walker (FLRW) cosmology. We shall summarize the essential features of this alternative model in Sect. 2, and then derive the growth equations in Sect. 2. We shall evaluate the halo mass function in Sects. 3 and 4, and end with our conclusions in Sect. 5.

2 The $R_{\rm h} = ct$ universe

The $R_{\rm h} = ct$ universe [17–22] has thus far been tested using a variety of observations. For a summary, see Table 2 in ref. [23]. The principal difference between ΛCDM and $R_{\rm h} = ct$ is that the latter model is constrained by the equation of state $\rho + 3p = 0$, i.e., the so-called zero active mass con-

dition in general relativity. In the standard model, radiation was dominant early, followed by matter and dark energy at later times, whereas dark energy has always been present in $R_{\rm h} = ct$, with a significant component of radiation early on, followed by matter towards lower redshifts. Also, the dark-energy equation of state is $w_{\rm de} = -1$ in ΛCDM, while it is $w_{\rm de} = -1/2$ in $R_{\rm h} = ct$ (see Ref. [24] for further details).

Some additional support for the $R_{\rm h} = ct$ cosmology, based on an alternative theoretical concept, may also be found in Ref. [25] and the updated discussion in Ref. [26]. But in spite of the success this model has enjoyed thus far in accounting for many observations as well, if not better, than the standard model, some counter claims have also been published in recent years, so the issue of whether or not it is the correct cosmology still needs to be resolved. This is a principal reason for continuing to test it as we do in this paper. Our analysis here advances this discussion significantly by providing new insights and an important new comparison between $R_{\rm h} = ct$ and ΛCDM using observations over an unusually large redshift range (see Figs. 2, 3, 4, 5, 6, 7 below).

As noted above, over the past decade, $R_{\rm h} = ct$ has been compared to ΛCDM using data across a broad redshift range, using integrated distances and the redshift-dependent Hubble parameter, among various other measures. Still, some of these data are often associated with unknown systematics and, worse, are often dependent on the presumed background model. The analysis of Type Ia SNe is a well-known example in which the lightcurve is characterized by at least 3 'nuisance' parameters that need to be optimized along with those in the cosmological model. A different choice of assumptions (e.g., the unknown intrinsic dispersions) and techniques (e.g., χ^2 minimization versus maximization of a likelihood function and/or model selection with information criteria), can sometimes produce varying outcomes in these tests.

For example, Type Ia SNe are challenging to use for model testing when various subsamples are merged together to improve the statistics, since one must deal with different unknown systematics in each case. In his assessment, Shafer [27] merged the Union2.1 and JLA samples and found that this compilation favours the standard model. In his analysis, however, he avoided the unknown intrinsic dispersions by instead constraining the reduced χ^2 to be 1 in each subsample. In recent years, a superior statistical approach has been developed [28–30] in which these unknowns are instead estimated by maximizing the overall likelihood function. The outcome of which cosmology is preferred by the SN data changes depending on which of these assumptions and methods are chosen.

Another recent test [31] used local probes, combining SN data with measurements of the Hubble parameter $H(z)$ and baryon acoustic oscillations (BAO). This analysis also showed that ΛCDM is favoured over $R_{\rm h} = ct$, contrasting with other work where the opposite was reported [30,32]. The

different results may be traced to the choice of data sets in the two studies. As is the case for SN measurements, the BAO also do not provide model-independent information since the location of the BAO peak cannot easily be distinguished from redshift space distortions (RSD). As of today, only 3 such measurements have provided a clean peak location. In other cases, a cosmology must be preassumed in order to model the RSD, rendering the data highly model-dependent. Any use of these BAO data, and the of $H(z)$ measured from them, produces a biased outcome. In their assessment, Lin et al. [31] used all the data and concluded, not surprisingly, that they favour ΛCDM because the standard model was used to estimate the RSD. When only model-independent data are used instead, however, one reaches the opposite conclusion [32].

As we discuss elsewhere in this paper, the inferred halo mass function is itself subject to an important unknown: the redshift dependence of the halo to stellar mass ratio M_h/M_*, so our conclusions may also require revision once new data will have been acquired. Depending on whether or not this ratio changes by roughly an order of magnitude between redshifts 4 and 10, a factor yet to be resolved observationally, ΛCDM may or may not be favoured over $R_{\rm h} = ct$. Nonetheless, providing one more important comparison between these two models is essential in establishing the conditions that must be met in order for $R_{\rm h} = ct$ to be viewed as a viable alternative to the standard model.

3 The Einstein–Boltzmann equations for dark matter and energy fluctuations

To obtain the complete evolution of density fields starting from initial perturbations, one must solve the coupled Boltzmann/Einstein equations (see Ref. [33]). The baryons are strongly coupled with radiation until decoupling and therefore do not contribute to the growth of structure during this epoch. Once they decouple from the radiation, baryons follow the evolution of dark matter, which has preceded them in forming bound systems. Hence, the initial growth of structure is dominated by dark matter. For this paper, which is focused on the question of halo growth, we therefore concentrate solely on the growth of dark matter perturbations. Other aspects of structure growth will be presented elsewhere [16]. Thus, since we are not interested here in temperature fluctuations of the radiation field or acoustic oscillations, we justify the use of Einstein–Boltzmann equations customized solely for the purpose of describing the growth of dark matter perturbations, which we derive as follows.

The distribution function for any species (i.e., dark matter, baryons, radiation, etc.) may depend on the coordinates (x^μ) and momentum (P^μ) 4-vectors, resulting in an 8-dimensional phase space. An additional constraint emerges,

however, from the invariant contraction of the momentum, $g_{\mu\nu} P^\mu P^\nu = -m^2$, which reduces the phase space to 7-dimensions. So we choose x^μ, $p \equiv |\boldsymbol{p}|$ and the direction of the momentum, $\hat{p}^i$, as our independent variables. Louisville's theorem produces the equation

$$\frac{df_s}{d\lambda} = \frac{\partial f_s}{\partial x^0}\frac{\partial x^0}{\partial \lambda} + \frac{\partial f_s}{\partial x^i}\frac{\partial x^i}{\partial \lambda} + \frac{\partial f_s}{\partial p}\frac{\partial p}{\partial \lambda}$$
$$+ \frac{\partial f_s}{\partial \hat{p}^i}\frac{\partial \hat{p}^i}{\partial \lambda} = C[f_s], \qquad (1)$$

where $f_s(x^\mu, p, \hat{p}^i)$ is the distribution function for any species 's' (i.e., dark matter, dark energy, baryons, etc.), λ is the affine parameter, and $C[f_s]$ is a collision/source term for this species. We define $P^\mu = dx^\mu/d\lambda$, so that $dx^0/d\lambda = P^0$. Dividing the above equation by P^0, and neglecting the fourth term that is of second order, gives

$$\frac{df_s}{d\eta} = \frac{\partial f_s}{\partial \eta} + \frac{\partial f_s}{\partial x^i}\frac{P^i}{P^0} + \frac{\partial f_s}{\partial p}\frac{\partial p}{\partial \eta} = \frac{C[f_s]}{P^0}, \qquad (2)$$

where η is now the conformal time, $d\eta \equiv dt/a(t)$, in terms of the expansion factor $a(t)$ and cosmic time t in the Friedmann–Lemaître–Robertson–Walker metric.

In the above equation, we may write $P^i/P^0 = (p/E)\hat{p}^i$ (where E is the energy) and, using the geodesic equation, we get

$$\frac{dp}{d\eta} = -\mathcal{H}p + E\hat{p}^l \partial_l \frac{h_{00}}{2} - \frac{p}{2}\frac{dh_{ij}}{d\eta}\hat{p}^i\hat{p}^j, \qquad (3)$$

where $\mathcal{H}$ is the Hubble parameter written in terms of η, and $h_{\alpha\beta}$ are the perturbed metric coefficients. Substituting Eq. (3) into Eq. (2), we get

$$\frac{df_s}{d\eta} + \frac{p\hat{p}^i}{E}\frac{\partial f_s}{\partial x^i} + p\left(-\mathcal{H} + \frac{E}{p}\hat{p}^l\partial_l\frac{h_{00}}{2} - \frac{1}{2}h'_{ij}\hat{p}^i\hat{p}^j\right)\frac{\partial f_s}{\partial p}$$
$$= \frac{a}{E}(1 - \Phi)C[f_s], \qquad (4)$$

where we have substituted $P_0 = \frac{E}{a}(1 + \Phi)$, in terms of the perturbed gravitational potential Φ. We now separate the distribution function into its unperturbed component, $\bar{f}_s$, and the perturbed contribution, $\mathcal{F}_s$, such that

$$f_s(\eta, x^i, p, \hat{p}^i) = \bar{f}_s(\eta, x^i, p, \hat{p}^i) + \mathcal{F}_s(\eta, x^i, p, \hat{p}^i). \quad (5)$$

Then, multiplying Eq. (4) by $E(p)$, and integrating over momentum space, collecting the zeroth-order terms, gives

$$\int \frac{d^3 p}{(2\pi)^3} E(p)\frac{d\bar{f}_s}{d\eta} - \int \frac{d^3 p}{(2\pi)^3}\mathcal{H}pE(p)\frac{\partial\bar{f}_s}{\partial p}$$
$$= \int \frac{d^3 p}{(2\pi)^3} aC[f_s]. \qquad (6)$$

In this expression, $C[f_s]$ is zero in the context of ΛCDM because the particle number is conserved during this phase of the fluctuation growth. But this is not the case in $R_{\rm h} = ct$. The early universe in this model contains approximately 80%

dark energy and approximately 20% radiation, with a small contamination of matter [24]. At late times, the $R_h = ct$ universe contains approximately 70% dark energy and 30% matter. A coupling therefore exists between dark matter and dark energy, such that the particle number for each individual species is not conserved in this model. The right-hand side of Eq. (6) is therefore not zero in $R_h = ct$. Integrating the second term on the left-hand side by parts and neglecting the boundary term, we arrive at the expression

$$\int \frac{d^3 p}{(2\pi)^3} E(p) \frac{d\bar{f}_s}{d\eta} + 3\mathcal{H} \int \frac{d^3 p}{(2\pi)^3} \left(E + \frac{p^2}{3E} \right) \bar{f}_s$$
$$= \int \frac{d^3 p}{(2\pi)^3} a C[f_s]. \tag{7}$$

This equation may be further reduced by using the following definitions for the (background) density and pressure:

$$\rho_s = \int \frac{d^3 p}{(2\pi)^3} E(p) \bar{f}_s, \tag{8}$$

and

$$\mathcal{P}_s = \int \frac{d^3 p}{(2\pi)^3} \frac{p^2}{3E} \bar{f}_s. \tag{9}$$

When applied to dark matter, Eq. (7) may thus be written as follows

$$\frac{d\rho_{\rm dm}}{d\eta} + 3\mathcal{H}(\rho_{\rm dm} + \mathcal{P}_{\rm dm}) = \int \frac{d^3 p}{(2\pi)^3} a C[f_{\rm dm}]. \tag{10}$$

For this particular species (i.e., dark matter), we may also put $\mathcal{P}_{\rm dm} = 0$. In addition, we use an approximate empirical expression, $\rho_{\rm dm} = (\rho_c/3a^2) \exp\left(-\frac{a_*}{a}\frac{(1-a)}{(1-a_*)}\right)$, to model the transition from a radiation/dark-energy dominated early universe to a matter/dark-energy dominated universe at late times, where ρ_c is the critical density today, and a_* represents the scale factor at matter radiation equality. Note that we are also normalizing $a(t_0)$ to be 1 today, which is possible in a spatially flat Universe. We infer the required collision/source term in Eq. (10) by using this empirical expression for $\rho_{\rm dm}$, which yields

$$\int \frac{d^3 p}{(2\pi)^3} a C[f_{\rm dm}] = \mathcal{H}\rho_{\rm dm} + \frac{H\rho_{\rm dm}}{a}\left(\frac{a_*}{1-a_*}\right). \tag{11}$$

It is not difficult to see that the above equation is satisfied to zeroth order only if

$$C[\bar{f}_{\rm dm}] = \frac{\mathcal{H}E}{a} \bar{f}_{\rm dm} + \frac{\mathcal{H}E}{a^2} \bar{f}_{\rm dm}\left(\frac{a_*}{1-a_*}\right). \tag{12}$$

This collision/source term explicitly shows the interactions between dark energy and dark matter required to sustain the zero active mass condition described above. That is, in order for the partitioning of 80% dark energy plus 20% radiation in the early Universe to transition to a balance of 70% dark energy plus 30% matter today, a fraction of the dark

energy must decay/evolve into dark matter. As such, the collision/source for dark energy must be the negative of Eq. (12), so that

$$\frac{d\rho_{\rm de}}{d\eta} + 3\mathcal{H}(\rho_{\rm de} + \mathcal{P}_{\rm de})$$
$$= -\int \frac{d^3 p}{(2\pi)^3} \left[\mathcal{H}E \bar{f}_{\rm dm} + \frac{\mathcal{H}E}{a} \bar{f}_{\rm dm}\left(\frac{a_*}{1-a_*}\right) \right], \tag{13}$$

where

$$C[\bar{f}_{\rm de}] = -\frac{\mathcal{H}E}{a} \bar{f}_{\rm dm} + \frac{\mathcal{H}E}{a^2} \bar{f}_{\rm dm}\left(\frac{a_*}{1-a_*}\right). \tag{14}$$

Returning now to Eq. (4), and using Eq. (12), we find for dark matter that

$$\frac{df_{\rm dm}}{d\eta} + \frac{p\hat{p}^i}{E} \frac{\partial f_{\rm dm}}{\partial x^i}$$
$$+ \left(-\mathcal{H} + \frac{E}{p}\hat{p}^l \partial_l \frac{h_{00}}{2} - \frac{1}{2}h'_{ij}\hat{p}^i\hat{p}^j \right) \frac{\partial f_{\rm dm}}{\partial p}$$
$$= \left[\mathcal{H}f_{\rm dm} + \frac{\mathcal{H}}{a} f_{\rm dm}\left(\frac{a_*}{1-a_*}\right) \right](1-\Phi) \tag{15}$$

We again multiply this equation by $E(p)$ and integrate over momentum space, but now collecting first order terms, finding that

$$\frac{d(\delta\rho_{\rm dm})}{d\eta} + (\rho_{\rm dm} + \mathcal{P}_{\rm dm})\partial_i v^i_{\rm dm} + 3\mathcal{H}(\delta\rho_{\rm dm}$$
$$+ \delta\mathcal{P}_{\rm dm}) + 3(\rho_{\rm dm} + \mathcal{P}_{\rm dm})\frac{d\Phi}{d\eta}$$
$$= \left[\mathcal{H} + \frac{\mathcal{H}}{a}\left(\frac{a_*}{1-a_*}\right) \right](1-\Phi)\delta\rho_{\rm dm} \tag{16}$$

where, as always, Φ is the gravitational potential. Then, defining $\delta_{\rm dm} \equiv \delta\rho_{\rm dm}/\rho_{\rm dm}$ for the dark-matter perturbation, with $\mathcal{P}_{\rm dm} = \delta\mathcal{P}_{\rm dm} = 0$, we may write

$$\frac{d\delta_{\rm dm}}{d\eta} = \frac{1}{\rho_{\rm dm}} \frac{d(\delta\rho_{\rm dm})}{d\eta} - \frac{\delta_{\rm dm}}{\rho_{\rm dm}} \frac{d\rho_{\rm dm}}{d\eta}. \tag{17}$$

Substituting for $d(\delta\rho_{\rm dm})/d\eta$ in Eq. (16), and isolating the Fourier mode k, we find that

$$\frac{d\delta_{{\rm dm},k}}{d\eta} = -ku_k - 3\frac{d\Phi_k}{d\eta} - \mathcal{H}\left[1 + \frac{a_*}{a(1-a_*)} \right]\Phi, \tag{18}$$

where we have written $\partial_i v^i_k = ku_k$, in terms of the velocity perturbation u_k of the dark matter. Finally, we take the second moment of Eq. (15), multiplying it by $p\hat{p}^i$ and contracting it with $i\hat{k}_i$. Then integrating over momentum space, and collecting first order terms, we get

$$\frac{d(\rho_{\rm dm}u_{{\rm dm},k})}{d\eta} + 4\mathcal{H}\rho_{\rm dm}u_{{\rm dm},k} + k\Phi\rho_{\rm dm}$$
$$= \mathcal{H}\left[1 + \frac{a_*}{a(1-a_*)} \right]\rho_{\rm dm}u_{{\rm dm},k}, \tag{19}$$

where $u_{\mathrm{dm,k}}$ is the kth velocity perturbation of dark matter. Substituting for $d\rho_{\mathrm{dm}}/d\eta$ in the above equation we thus get

$$\frac{du_{\mathrm{dm,k}}}{d\eta} = -\frac{1}{a}\frac{da}{d\eta}u_{\mathrm{dm,k}} - k\Phi_k. \tag{20}$$

Turning now to the dark-energy perturbations, we begin with Eq. (4) and the interaction term in Eq. (14), and find that

$$\frac{df_{\mathrm{de}}}{d\eta} + \frac{p\hat{p}^i}{E}\frac{\partial f_{\mathrm{de}}}{\partial x^i} + p\left(-\mathcal{H} + \frac{E}{p}\hat{p}^l\partial_l\frac{h_{00}}{2} - \frac{1}{2}h'_{ij}\hat{p}^i\hat{p}^j\right)$$
$$\frac{\partial f_{\mathrm{de}}}{\partial p} = -\mathcal{H}(1-\Phi)\left[1 + \frac{a_*}{a(1-a_*)}\right]f_{\mathrm{dm}}, \tag{21}$$

where f_{de} is the distribution function for dark-energy. Thus, partitioning f_{de} into its unperturbed ($\bar{f}_{\mathrm{de}}$) and perturbed ($\mathcal{F}_{\mathrm{de}}$) components, as was done in Eq. (5), we can collect the first-order perturbed terms to find that

$$\frac{d\mathcal{F}_{\mathrm{de}}}{d\eta} + \frac{p\hat{p}^i}{E}\frac{\partial\mathcal{F}_{\mathrm{de}}}{\partial x^i} - \mathcal{H}p\frac{\partial\mathcal{F}_{\mathrm{de}}}{\partial p} + p\left(\frac{E}{p}\hat{p}^l\partial_l\frac{h_{00}}{2}\right.$$
$$\left. -\frac{1}{2}h'_{ij}\hat{p}^i\hat{p}^j\right)\frac{\partial\bar{f}_{\mathrm{de}}}{\partial p} = -\mathcal{H}\left[1 + \frac{a_*}{a(1-a_*)}\right]$$
$$\left(\mathcal{F}_{\mathrm{dm}} - \Phi\bar{f}_{\mathrm{dm}}\right). \tag{22}$$

Multiplying this equation by $E(p)$ and integrating over the momentum space then gives

$$\frac{d\delta\rho_{\mathrm{de}}}{d\eta} + \rho_{\mathrm{de}}(1+w_{\mathrm{de}})ku_{\mathrm{de,k}} + 3\mathcal{H}\delta\rho_{\mathrm{de}}\left(1 + \frac{\delta\mathcal{P}_{\mathrm{de}}}{\delta\rho_{\mathrm{de}}}\right)$$
$$+3\frac{d\Phi}{d\eta}\rho_{\mathrm{de}}(1+w_{\mathrm{de}}) = \mathcal{H}\left[1 + \frac{a_*}{a(1-a_*)}\right](\rho_{\mathrm{dm}}\Phi - \delta\rho_{\mathrm{dm}}). \tag{23}$$

Defining $\delta_{\mathrm{de}} = \delta\rho_{\mathrm{de}}/\rho_{\mathrm{de}}$, and using $\mathcal{P}_{\mathrm{de}} = -\rho_{\mathrm{de}}/2$ ([24]) we may write

$$\frac{d\delta_{\mathrm{de}}}{d\eta} = \frac{1}{\rho_{\mathrm{de}}}\frac{d\delta\rho_{\mathrm{de}}}{d\eta} - \frac{\delta\rho_{\mathrm{de}}}{\rho_{\mathrm{de}}^2}\frac{d\rho_{\mathrm{de}}}{d\eta}, \tag{24}$$

so that with Eqs. (13) and (23), we find that

$$\frac{d\delta_{\mathrm{de}}}{d\eta} = -\frac{k}{2}u_{\mathrm{de,k}} - 3\mathcal{H}\delta_{\mathrm{de}}\left(\frac{1}{2} + \frac{\delta\mathcal{P}_{\mathrm{de}}}{\delta\rho_{\mathrm{de}}}\right) - \frac{3}{2}\frac{d\Phi}{d\eta}$$
$$+\mathcal{H}\left[1 + \frac{a_*}{a(1-a_*)}\right]\frac{\rho_{\mathrm{dm}}}{\rho_{\mathrm{de}}}(\delta_{\mathrm{de}} - \delta_{\mathrm{dm}} + \Phi). \tag{25}$$

The sound speed for our coupled dark matter/dark energy fluid is not known yet, so we write it as follows

$$c_s^2 \equiv \frac{\delta\mathcal{P}}{\delta\rho} = \frac{\delta\mathcal{P}_{\mathrm{de}}}{\delta\rho_{\mathrm{dm}} + \delta\rho_{\mathrm{de}}} = \frac{\delta\mathcal{P}_{\mathrm{de}}/\delta\rho_{\mathrm{de}}}{(1 + \delta\rho_{\mathrm{dm}}/\delta + \rho_{\mathrm{de}})}, \tag{26}$$

analogously to what is commonly done with the coupled baryon-radiation fluid in the standard model. And following the conventional approach of assuming adiabatic fluctu-

ations, we also write

$$\frac{\delta\mathcal{P}_{\mathrm{de}}}{\delta\rho_{\mathrm{de}}} = c_s^2\left[1 + \frac{2\rho_{\mathrm{dm}}}{\rho_{\mathrm{de}}}\right]. \tag{27}$$

For the sake of simplicity, we assume the sound speed to be a constant delimited to the range $0 \lesssim (c_s/c)^2 \lesssim 1$. We have found that the actual value of this constant has a negligible impact on the solutions to the above equations since the ratio of dark matter density to dark energy is always much less than 1 in the $R_{\mathrm{h}} = ct$ universe, and we therefore adopt the simple fraction $c_s^2 = c^2/2$ throughout this work. Thus, using Eqs. (25) and (27), we get

$$\frac{d\delta_{\mathrm{de}}}{d\eta} = -\frac{k}{2}u_{\mathrm{de,k}} - \delta_{\mathrm{de}}\left(\frac{3\mathcal{H}}{2} + 3\mathcal{H}c_s^2 + \frac{6\mathcal{H}c_s^2\rho_{\mathrm{dm}}}{\rho_{\mathrm{de}}}\right)$$
$$-\frac{3}{2}\frac{d\Phi}{d\eta} + \mathcal{H}\left[1 + \frac{a_*}{a(1-a_*)}\right]\frac{\rho_{\mathrm{dm}}}{\rho_{\mathrm{de}}}(\delta_{\mathrm{de}} - \delta_{\mathrm{dm}} + \Phi). \tag{28}$$

Finally, we take the second moment of Eq. (21), multiply it by $p\hat{p}^i$ and contract it with $i\hat{k}_i$. Integrating over momentum space, and collecting first order terms, we thus find that

$$\frac{du_{\mathrm{de,k}}}{d\eta} = -\frac{5\mathcal{H}}{2}u_{\mathrm{de,k}} - k\Phi + 2kc_s^2\left[1 + \frac{2\rho_{\mathrm{dm}}}{\rho_{\mathrm{de}}}\right]\delta_{\mathrm{de}}$$
$$+\mathcal{H}\left[1 + \frac{a_*}{a(1-a_*)}\right]\frac{\rho_{\mathrm{dm}}}{\rho_{\mathrm{de}}}(u_{\mathrm{de,k}} - 2u_{\mathrm{dm,k}}). \tag{29}$$

Our final equation comes from perturbing the FLRW metric in Einstein's equations (see [33]), which gives

$$k^2\Phi_k + 3\frac{1}{a}\frac{da}{d\eta}\left(\frac{d\Phi_k}{d\eta} + \frac{1}{a}\frac{da}{d\eta}\Phi_k\right)$$
$$= 4\pi Ga^2\left[\rho_{\mathrm{m}}\delta_{\mathrm{dm,k}} + \rho_{\mathrm{de}}\delta_{\mathrm{de}}\right]. \tag{30}$$

In arriving at Eq. (30), we have chosen the Newtonian gauge for the primary reason that the independent components in this gauge have a direct correspondence to the gauge invariant Bardeen variables [33,34].

It is important to stress that the set of Eqs. (18), (20), (28) and (29) in $R_{\mathrm{h}} = ct$ differ from their counterparts in ΛCDM. This happens because dark energy and dark matter are coupled in $R_{\mathrm{h}} = ct$, while dark energy is simply a cosmological constant in the most basic ΛCDM model. The only expression that is formally common to both $R_{\mathrm{h}} = ct$ and ΛCDM is Eq. (20), though the dependence of ρ_{dm} on $a(t)$ is, of course, model dependent. Mathematically, this comes about because the collision/source term in Eq. (12) actually cancels out in the perturbation Eq. (19) for the velocity perturbations. The dependence on cosmology also enters into the growth of δ_{dm} via the model-dependent $\mathcal{H}$ and $a(t)$ functions. These quantities change with time according to the background evolution, and are therefore strongly dependent on the chosen model.

More specifically, an inspection of these equations reveals that there are three principal differences between $R_h = ct$ and ΛCDM: (1) the scale factor $a(t)$ in $R_h = ct$ is given as $a(t) = (t/t_0)$ at all epochs, whereas in ΛCDM it is proportional to $t^{1/2}$ and $t^{2/3}$ during the radiation and matter dominated phases, respectively; (2) the matter density scales as $\rho_{dm} = (\rho_c/3a^2) \exp\left(-\frac{a_*}{a}\frac{(1-a)}{(1-a_*)}\right)$ in $R_h = ct$, whereas it is given as $\rho_m = (\Omega_m \rho_c / a^3)$ in ΛCDM; and (3) the various modes of the density field in ΛCDM exited the horizon during inflation, whereas none of the modes ever crossed the horizon in $R_h = ct$ [49]. In ΛCDM, small-scale modes re-entered the horizon while radiation was dominant, while larger-scale modes entered the horizon when matter dominated, which produces a late start for the growth of structure compared with what happens in $R_h = ct$. This appears to be the principal reason why galaxies and supermassive black holes appeared earlier in $R_h = ct$ than in the standard model.

We shall formally introduce the growth function in Eq. (31) below, and plot it in Fig. 1. It is obtained by solving Eqs. (10)–(30) simultaneously (see Ref. [16] for more details). It is quite evident from this plot that the growth factor in $R_h = ct$ is significantly stronger at large redshifts than that in ΛCDM, in full agreement with the previous results of our analysis at lower redshifts [35]. In contrast, the growth function in ΛCDM indicates a strong evolution from $z \sim 10$ to $z \sim 4$. And since galaxies typically form on a dynamical timescale ~ 300 Myr [36] after halo virialization, the rapid evolution in the number density of halos from $z \sim 8$ to ~ 4 predicted by ΛCDM corresponds to a rapid evolution in the UV luminosity of galaxies at $6.0 \gtrsim z \gtrsim 3.4$. This is one of the points of contention between the two camps, since this (required) rapid evolution in the UV luminosity function conflicts with the observations [9]. The observed UV luminosity evolves much more slowly than this prediction, which would mean that these massive galaxies would have formed much earlier than expected in ΛCDM.
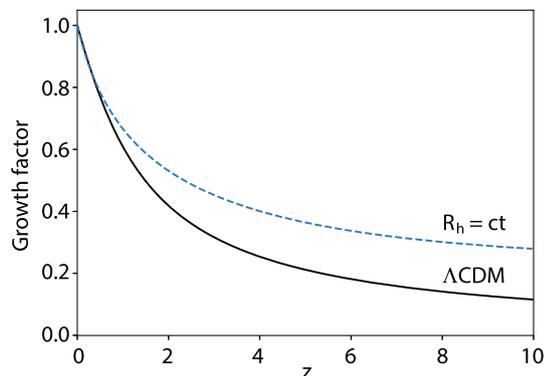
4 Halo mass function

The halo mass function was first derived by Press and Schechter [37] assuming spherical collapse and a primordial Gaussian density field. When tested against numerical simulations, however, it became evident that the Press-Schechter formalism over-predicts the number of halos at the high mass end, and under-predicts at the low mass end. This inconsistency was resolved by introducing ellipsoidal collapse, rather than spherical, by Sheth–Tormen [1]. But the Bolshoi simulations performed by Klypin et al. [38] several years later indicated that, while discrepancies in the Sheth–Tormen mass function at $z \sim 0$ are less than 10% for halo masses in the range $5 \times 10^9 - 5 \times 10^{14}$ $M_\odot$, this prescription over-predicts the density by about 50% at $z \sim 6$ for masses in the range $10^{11} - 10^{12}$ $M_\odot$, getting even worse (by an order of magnitude) by $z \sim 10$. Unfortunately for the standard model, the inclusion of corrections from the Bolshoi simulations actually exacerbates the discrepancy between theory and observation. For this reason, and the fact that analogous simulations to the Bolshoi calculations have not yet been carried out for $R_h = ct$, we won't include such adjustments in this paper. We point out that if we were to add such corrections to $R_h = ct$, the comparison of this model's predictions with the data under the assumption of a constant halo mass to stellar mass ratio would be even more favourable than the Sheth–Tormen formulation on its own, as one may readily see in Figs. 2, 3, 4, 5, 6 and 7. As such, our exclusion of these corrections produces an effect more favourable to ΛCDM than $R_h = ct$, even with this assumption, which we do in order give the standard model as much benefit of the doubt as possible.

Fig. 1 Growth Factor predicted by $R_h = ct$ (dashed) and flat ΛCDM (solid)
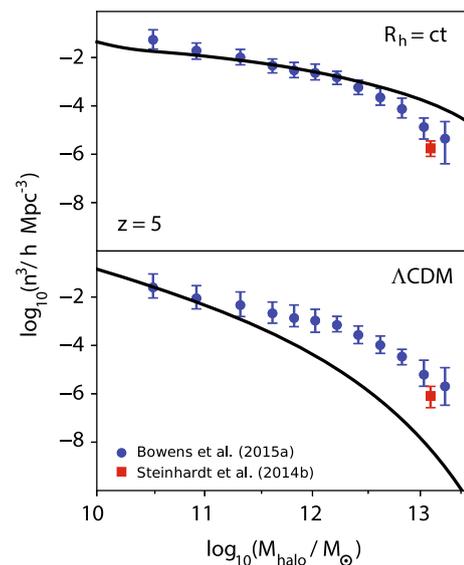
Fig. 2 Top: halo mass function inferred from galaxy surveys at $z = 5$ compared with $R_h = ct$. Bottom: same, except now for ΛCDM
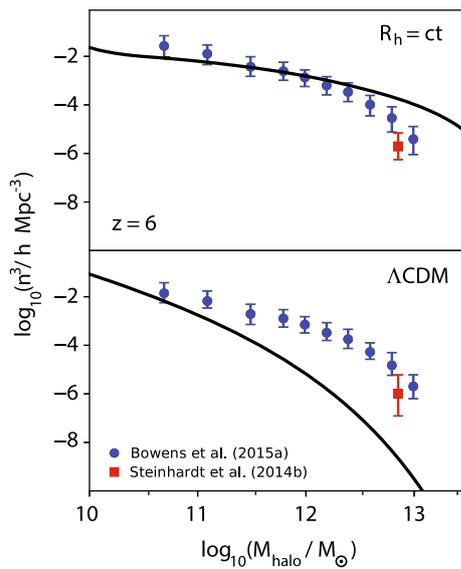
Fig. 3 Top: halo mass function inferred from galaxy surveys at $z = 6$ compared with $R_h = ct$. Bottom: same, except now for ΛCDM
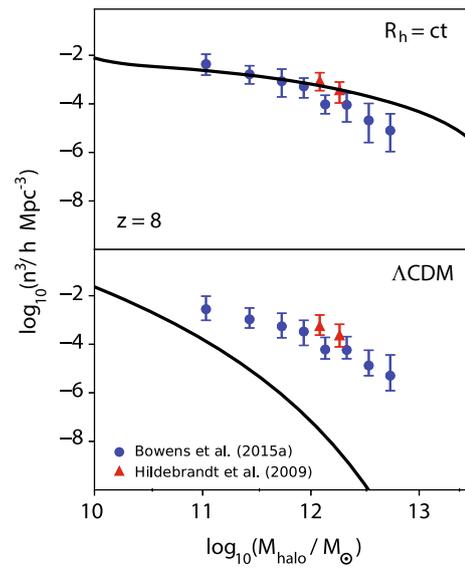
Fig. 5 Top: halo mass function inferred from galaxy surveys at $z = 8$ compared with $R_h = ct$. Bottom: same, except now for ΛCDM
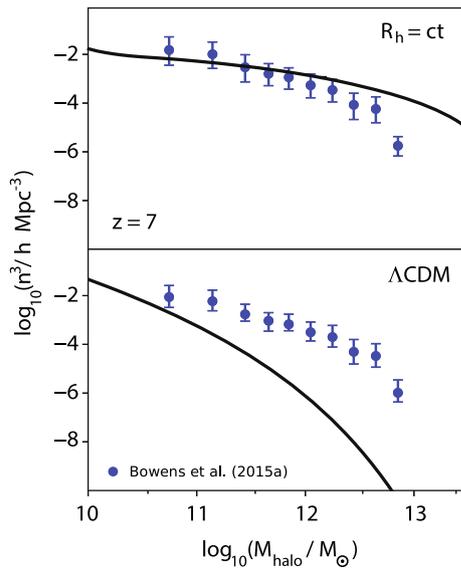
Fig. 4 Top: halo mass function inferred from galaxy surveys at $z = 7$ compared with $R_h = ct$. Bottom: same, except now for ΛCDM
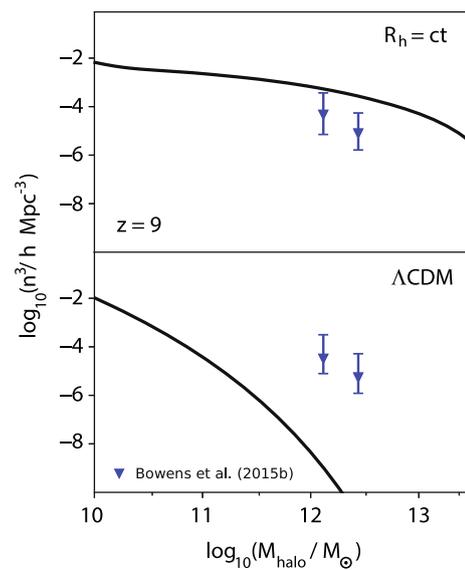
Fig. 6 Top: halo mass function inferred from galaxy surveys at $z = 9$ compared with $R_h = ct$. Bottom: same, except now for ΛCDM

The Sheth–Tormen mass function is given as

$$f(\sigma) = A \sqrt{\frac{2a}{\pi}} \left[1 + \left(\frac{\sigma^2}{a\delta_c^2} \right)^p \right] \frac{\delta_c}{\sigma} \exp \left[-\frac{a\delta_c^2}{2\sigma^2} \right], \qquad (31)$$

where $A = 0.3222$ is a normalization factor, and $a = 0.707$ and $p = 0.3$. Using this halo mass function, one may obtain the number of dark matter halos per comoving volume with masses less than M as follows:

$$\frac{dn}{d \ln M} = \frac{\rho_0}{M} f(\sigma) \left| \frac{d \ln \sigma}{d \ln M} \right|, \qquad (32)$$

where σ is defined according to the expression

$$\sigma_R^2(R, z) = \frac{b^2(z)}{2\pi^2} \int_0^\infty k^2 P(k) W^2(k, R) dk, \qquad (33)$$

and $P(k)$ is the power spectrum, $W(k, R)$ is the top-hat filter and $b(z)$ is the growth factor shown in Fig. 1 for both ΛCDM and $R_h = ct$.
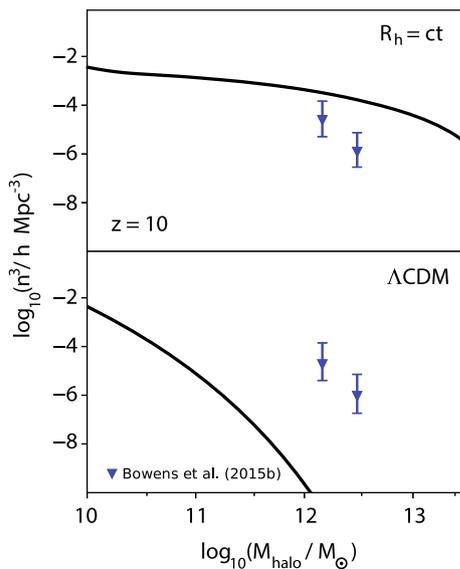
Fig. 7 Top: halo mass function inferred from galaxy surveys at $z = 10$ compared with $R_h = ct$. Bottom: same, except now for ΛCDM

5 Observed halo mass function

The data used in this paper were assembled by Steinhardt et al. [9], based on measurements obtained using three different techniques, including the clustering method [39,43] based on the spatial distribution of galaxies to obtain the halo masses. This method doesn't assume any physical properties of the galaxies themselves, but assumes a model for the dark matter concentration. Other techniques include template fitting [40], that adopts a relationship between the luminosity and stellar masses; the abundance matching technique [13] that relates critical features in the galaxy luminosity or mass function, such as a 'knee', to crucial elements in the halo mass distribution, that can then be used to match the galaxy and dark matter densities to infer the halo mass function. The high redshift ($z \gtrsim 6$) data points are derived from the UV luminosity function, that yields halo masses by assuming that the halo mass to light ratio obtained at lower redshifts persists to higher redshifts. Most of the data used in this work were obtained assuming a constant ratio of halo to stellar-mass. The two main principles for arriving at this ratio are (1) that 10% of the baryonic matter eventually condensed into stars [41] and (2) the observation of a 6:1 ratio of dark matter to baryonic matter [42].

It is quite obvious from the progression seen in Figs. 2, 3, 4, 5, 6 and 7 that the observed halo mass function obtained via these different techniques [13,39,43,44] is entirely inconsistent with the distribution predicted by ΛCDM, if the halo to stellar-mass ratio remains constant throughout the $4 \lesssim z \lesssim 10$ redshift range [9]. Of course, the caveat is that these data were not measured directly, and were obtained using relationships derived at low redshifts. Steinhardt et al.

[9] studied the possibility that these correlations could be breaking down at high-z. Their investigation indicated, however, that the star-formation rate vs. stellar mass of these high redshift galaxies lies on the extrapolation from lower redshift galaxies. In addition, the ratio of stellar mass to halo mass in these high redshift galaxies is similar to the standard value 30:1 seen at all redshifts. These two tests therefore indicate that the high redshift galaxies are quite normal, implying that the problem is real.

In addition to this, Steinhardt et al. [9] determined that an evolution of 0.8 dex in M_{Halo}/L_{UV} is needed to mitigate this problem. Such a change might occur if the stellar population in galaxies at $z = 8$ is younger than that at $z = 4$. Steinhardt et al. [9] extensively investigated whether this possibility could mitigate the disparity by modeling the halo mass to light ratio from an initial stellar population assuming they formed in one rapid burst at $z = 12$ and then evolved along the main sequence until $z = 4 - 8$, where they were observed. This resulted in a star formation rate $\propto M_*^{0.7}$, with a stellar age asymptotically approaching $50 - 150$ Myr, starting from an initially small value. But this isn't sufficient enough to remove the problem and, worse, the above approach isn't realistic considering a dynamical timescale of 300 Myr for star formation after virialization of the halo.

Steinhardt et al. [9] considered this scenario and modeled the halo mass to light ratio as described above, concluding that this too is insufficient to reconcile the problem. Another possibility is that the halo mass to stellar mass ratio evolves towards higher redshifts. An evolution of 0.8 dex in this ratio would reconcile the problem. But such a modification is only possible either by a complete absence of dark matter at redshift 8, or if 100% of the baryons condensed instantly into stars at high redshift upon halo virialization, which is quite impossible. Hence, one may reasonably conclude that this problem may be reconciled in ΛCDM only via the introduction of implausible physics. When viewed in the context of other "too early" types of problems, the disparity evident in Figs. 2, 3, 4, 5, 6 and 7 is quite damning for the standard model. For example, the early appearance of supermassive black holes at $z \sim 6$–7 [45,46] and galaxies at $z \sim 10 - 12$ (see references cited in [47], argues in favor of these problems being real, presenting a challenge to any attempt to alleviate them in the context of ΛCDM.

In contrast, the comparison between the Steinhardt et al. [9] data, under the assumption that the halo to stellar mass ratio is constant in the redshift range $4 \lesssim z \lesssim 10$, and the predictions of $R_h = ct$, is very favourable – except at the very high mass end of the halo mass distribution, as one may see in Figs. 2, 3, 4, 5, 6 and 7. The standard model disagrees progressively more and more with this approach as the redshift increases, while $R_h = ct$ fits the data throughout the range $10 \gtrsim z \gtrsim 4$ very well at the low and intermediate mass end, and overpredicts by one to two orders of mag-

nitude at the high mass end. This over-prediction may be due to two possible reasons: (1) as noted earlier, the Bolshoi simulation [38] has indicated that the Sheth–Tormen mass function overpredicts the number of halos by at least 10% at redshift $z \sim 0$, and overpredicts by at least 50% at redshift $z \sim 10$. Although simulations similar to Bolshoi haven't yet been carried out for $R_h = ct$, a trend analogous to this in the context of this model, would produce corrections that largely mitigate the problem at the high mass end; (2) this over-prediction may also be due in part to observational selection effects that may be 'hiding' some of the sources. Some massive galaxies may have been missed due to extinction, which future observations might be able to address. Regardless of which, if any, of these mitigating factors are at play in $R_h = ct$, none of them can resolve the disparity arising from the predictions of ΛCDM. The discrepancy seen in the standard model is extreme, ranging from one to over four orders of magnitude from low to high mass, throughout the redshift range $4 \lesssim z \lesssim 10$. The factors that may alleviate the high-mass end problem with $R_h = ct$, actually makes the comparison much worse for ΛCDM, increasing the disparity between predictions and observations. The weaker evolution in growth rate predicted by $R_h = ct$ is the vital reason for its success, indicating that massive galaxies must have formed earlier than predicted in the standard model, consistent with the observations.

The problem in ΛCDM may instead be reconciled with an evolution in the halo mass to light ratio, which could happen, e.g., if the initial mass function were top-heavy. Studies have shown, however, that this function should be the same at all redshifts $z \lesssim 8$ [48]. Hopefully, this conclusion can be tested using supernova rates in the future, which may eliminate even this last possible caveat for the significant tension between the observed halo mass function and ΛCDM. On the flip side, if it turns out that future observations with JWST support an evolution in the halo to stellar mass ratio of at least ~ 0.8 dex between $z \sim 4$ and 10, validating the predictions of ΛCDM, the inferred halo distribution will be in tension with the predictions of $R_h = ct$. The differences are so significant (at least several orders of magnitude) that a refinement of the halo distribution may produce one of the most robust comparative cosmological tests of these models.

6 Conclusion

In this paper, we have discussed an ongoing debate concerning the early appearance of massive galaxies (and their halos), which may challenge the formation of structure predicted by ΛCDM if the halo to stellar mass ratio is roughly constant in the redshift range $4 \lesssim z \lesssim 10$. This difficulty could be mitigated with a refinement of the underlying theory of star formation and galaxy evolution, but appears to

require implausible modifications to the physics underlying these phenomena (Steinhardt et al. 2016). Some support for the existence of a real problem is provided by other types of "too early" problems, such as the premature appearance of supermassive black holes at $z \sim 6$–7 [45,46].

Combining our earlier measurement of σ_8 at redshift 0 [49] with our recently completed calculation of the growth function using the coupled Boltzmann and perturbed Einstein equations, we have re-analyzed "The Impossibly Early Galaxy Problem" in the context of $R_h = ct$ and showed that this problem virtually disappears in this cosmology even if the halo to stellar mass ratio is constant. Although, the $R_h = ct$ universe overpredicts the number density of halos by one to two orders of magnitude at the very high mass end, this problem may be mitigated by corrections to the Sheth–Tormen mass function, as indicated by the Bolshoi simulations [38]. Thus, once we resolve the question of whether or not this ratio evolved with redshift, the inferred halo mass distribution can clearly distinguish between the $R_h = ct$ and ΛCDM cosmologies.

The timeline in $R_h = ct$ allows both massive galaxies and supermassive black holes to form at very high redshifts without invoking exotic physics. It should also be noted that, while ΛCDM must rely on the unproven and as yet unverified physics of inflation to account for the generation of scale-invariant primordial fluctuations and a mechanism for driving the modes to exit and re-enter the horizon, thus creating an intricate mechanism for producing different growth rates at different epochs, no such complicated, fine-tuned mechanism is necessary in $R_h = ct$. This model does not have a horizon problem and does not incorporate inflation into its expansion history. As explained in more detail in Ref. [16], the growth of structure in $R_h = ct$ is simple, streamlined and does not require a different handling of small modes compared to the larger ones. Such simplicity, particularly when viewed in the context of the excellent agreement between theory and observations (Figs. 2, 3, 4, 5, 6, 7), adds considerable support for the viability of this cosmology.

Looking forward to upcoming surveys and further theoretical developments, it is already clear that observations, e.g., with JWST, will play a crucial role in determining the quasar distribution and the rate of gamma ray bursts from Pop III stars, both heavily dependent on the growth rates we have been discussing in this paper. There is therefore significant promise of improving the comparison we have made here even further, perhaps strongly ruling out one or other of these two models.

References

1. R.K. Sheth, H.J. Mo, G. Tormen, MNRAS **323**, 1 (2001)
2. V. Springel et al., Nature **435**, 629 (2005)
3. M. Vogelsberger et al., MNRAS **444**, 1518 (2014)
4. G. Holder, Z. Haiman, J. Mohr, ApJ **560**, L111 (2001)
5. S.R. Furlanetto, M. McQuinn, L. Hernquist, MNRAS **365**, 115 (2006)
6. Z. Haiman, A. Loeb, ApJ **552**, 459 (2001)
7. N.A. Grogin et al., ApJ **197**, 35G (2011)
8. P. Capak et al., A&A **558**, 67A (2013)
9. C.L. Steinhardt, P. Capak, D. Masters, J.S. Speagle, APJ **824**, 1 (2016)
10. P.S. Behroozi, R.H. Wechsler, C. Conroy, APJL **762**, L31 (2013)
11. P.S. Behroozi, R.H. Wechsler, C. Conroy, APJ **770**, 57 (2013)
12. P.S. Behroozi, J. Silk, ApJ **799**, 32 (2015)
13. S.L. Finkelstein et al., ApJ **814**, 95 (2015)
14. A. Rodríguez-Puebla, J.R. Primack, V. Avila-Reese, S.M. Faber, MNRAS **470**, 651 (2017)
15. M. Stefanon et al., ApJ **843**, 36 (2017)
16. M.K. Yennapureddy, F. Melia, PRD (to be submitted) (2019)
17. F. Melia, MNRAS **382**, 1917 (2007)
18. F. Melia, A&A **553**, A76 (2013)
19. F. Melia, Front. Phys. **11**, 119801 (2016)
20. F. Melia, Front. Phys. **12**, 121980 (2017)
21. F. Melia, M. Abdelqader, IJMP-D **18**, 1889 (2009)
22. F. Melia, A.S.H. Shevchuk, MNRAS **419**, 2579 (2012)
23. F. Melia, MNRAS **481**, 4855 (2018)
24. F. Melia, M. Fatuzzo, MNRAS **456**, 3422 (2016)
25. M.V. John, K.B. Joseph, PRD **61**, 087304 (2000)
26. M.V. John, MNRAS **484**, L35 (2019)
27. D.L. Shafer, PRD **91**, 103516 (2015)
28. A.G. Kim, Publ. Astron. Soc. Pac. **123**, 230 (2011)
29. J.-J. Wei, X. Wu, F. Melia, R.S. Maier, AJ **149**, 102 (2015)
30. F. Melia et al., EPL **123**, 59002 (2018)
31. H.-N. Lin, X. Li, Y. Sang, Chin. Phys. C **42**, 095101 (2018)
32. F. Melia, M. López-Corredoira, IJMP-D **26**, 1750055 (2017)
33. C.P. Ma, E. Bertschinger, ApJ **455**, 7 (1995)
34. J.M. Bardeen, PRD **22**, 1882B (1980)
35. M.K. Yennapureddy, F. Melia, PDU **20**, 65Y (2018)
36. T. Wong, ApJ **705**, 650 (2009)
37. W. Press, P. Schechter, ApJ **187**, 425 (1974)
38. A.A. Klypin, S. Trujillo-Gomez, J. Primack, ApJ **740**, 102 (2011)
39. H. Hildebrandt, J. Pielorz, T. Erben, L. Van Waerbeke, P. Simon, P. Capak, A&A **498**, 725 (2009)
40. O. Ilbert et al., A&A **556**, A55 (2013)
41. A. Leauthaud et al., ApJ **744**, 159 (2012)
42. Planck Collaboration et al., A&A **594**, A13 (2016)
43. K.S. Lee et al., ApJ **752**, 66 (2012)
44. K.I. Caputi et al., ApJ **810**, 73 (2015)
45. F. Melia, ApJ **764**, 72 (2013)
46. F. Melia, T.M. McClintock, Proc. R. Soc. A **471**, 20150449 (2015)
47. F. Melia, JCAP **01**, 027 (2014)
48. B. Dias, P. Coelho, B. Barbuy, L. Kerber, T. Idiart, A&A **520**, A85 (2010)
49. F. Melia, MNRAS **464**, 1966 (2017)